COSINUS: A NaI-based cryogenic calorimeter for direct dark matter search

V. Zema([1])([2])([3]) on behalf of the COSINUS Collaboration

([1]) *GSSI, Gran Sasso Science Institute - L'Aquila, Italy*
([2]) *INFN, Laboratori Nazionali del Gran Sasso - Assergi, Italy*
([3]) *Chalmers University of Technology, Department of Physics - Göteborg, Sweden*

Summary. — For two decades, extraordinary effort has been devoted to clarifying the controversial results in direct dark matter detection. The claim of DAMA/LIBRA for a dark matter annual modulation signal is in apparent contradiction with most of the results of the other direct detection experiments, but a material-independent check of this signal can still be decisive. For this reason, COSINUS aims to develop a sodium iodide-based cryogenic scintillating calorimeter, whose two-channel readout of light and phonon allows an event-by-event discrimination of the dominant β/γ-background from the sought-for nuclear recoils.

1. – Introduction

Any scientific result requires severe tests before being accepted as a new contribution to knowledge. More than 20 years ago, the experiment DArkMAtter (DAMA) [1] was realised for the search of hypothetic particles supposed to be the content of the dark halo surrounding the galaxy [2]. After a brief period of data taking, during the TAUP conference held in 1997 at the Gran Sasso National Laboratory (L'Aquila, Italy) the collaboration released data showing the detection of a signal compatible with the expectations for dark matter [3]. The experiment has been running since that time and also the most recent data release confirms detection [4]. Experiments exploiting different techniques probed the dark matter parameter space and, according to the DAMA result, the claim of a positive signal looked right around the corner and would have provided unambiguous proof of the detection of dark matter. Despite of the extraordinary effort and the development of cutting edge technologies, the DAMA detection has not been confirmed by any experiment [5-13] and has been excluded in some scenarios [14, 15]. At the same time, all attempts for alternative explanations of the signal are excluded according to the DAMA Collaboration (*e.g.*, [16-19]). The exigency of testing this result motivated the construction of numerous experiments based on the same technology

as the DAMA setup for a completely model-independent check [20-23]. The COSINUS experiment participates in this campaign and benefits from the two-channel cryogenic technique for discriminating the potential signal from the background, a unique feature which sets it apart from the other sodium iodide-based experiments. Section **2** introduces the theoretical background for the direct dark matter search, sect. **3** discusses the COS-INUS scientific motivation, sects. **4** and **5** focus on the COSINUS experimental concept and on the experimental results obtained, sect. **6** presents status and perspectives and, finally, sect. **7** contains a brief conclusion.

2. – Theoretical assumptions for the dark matter particle search

2˙1. *Dark matter galactic halo.* – The standard framework underlying the direct dark matter particle search assumes that the galaxy is surrounded by a halo of collisionless, non-baryonic particles, in average at rest in the galactic rest frame. The shape and the mass density distribution of the galactic dark halo depends on the galaxy formation history. The simplest approximation is to consider an isothermal spherical halo, commonly named as Standard Halo Model (SHM) [24]. As a consequence, the kinematics of dark matter particles is described by a Maxwell-Boltzmann velocity distribution [25] truncated at the escape velocity $\mathbf{v}_{esc}$, that in the laboratory reference frame reads

$$(1) \qquad f(\mathbf{v}, \mathbf{v}_{obs}(t)) = \begin{cases} \dfrac{1}{N_{esc}} \left(\dfrac{1}{\pi v_0^2}\right)^{3/2} \exp[-(\mathbf{v} + \mathbf{v}_{obs}(t))^2 / v_0^2], & \text{for } |\mathbf{v} + \mathbf{v}_{obs}| < v_{esc}, \\ 0, & \text{otherwise}, \end{cases}$$

where $N_{esc} = \text{erf}[z] - (2/\sqrt{\pi})z e^{-z^2}$, with $z = v_{esc}/v_0$, $v_0 \simeq 220\,\text{km/s}$ is the most probable speed and $\mathbf{v}_{obs}(t)$ is the Earth velocity in the galactic rest frame, that is

$$(2) \qquad \mathbf{v}_{obs}(t) = \mathbf{v}_\odot + \mathbf{V}_\oplus(t),$$

with $\mathbf{v}_\odot \simeq (11, 232, 7)\,\text{km/s}$, and $\mathbf{V}_\oplus(t)$ being the Earth revolution velocity around the Sun.

2˙2. *Dark matter event rate annual modulation.* – The motion of Earth generates a relative velocity between a detector on Earth and the dark matter particles in the halo. The expected differential energy spectrum per unit of detector mass and per day is

$$(3) \qquad \frac{\mathrm{d}R}{\mathrm{d}E_R} = \frac{\rho_0}{m_\chi m_T} \int_{|\mathbf{V}| > v_{min}}^{|\mathbf{V} + \mathbf{V}_{obs}| < v_{esc}} \mathrm{d}\mathbf{v}\, \mathbf{v} f(\mathbf{v}, \mathbf{v}_{obs}(t)) \frac{\mathrm{d}\sigma}{\mathrm{d}E_R}(E_R, \mathbf{v}),$$

where E_R is the nucleus recoil energy, ρ_0 the dark matter mass density at the solar system distance from the galactic center, m_χ the dark matter mass, m_T the nucleus mass in GeV/c^2, which must be converted in kg to get the right dimensional units, v_{min} the minimal velocity required to produce a recoil energy E_R, v_{esc} the maximum velocity for particles trapped in the gravitational field of the galaxy, $\mathbf{v}_{obs}$ and $f(\mathbf{v}, \mathbf{v}_{obs}(t))$ are defined in eqs. (1) and (2). The velocity dependence of the differential dark matter-nucleus cross section $\frac{\mathrm{d}\sigma}{\mathrm{d}E_R}(E_R, \mathbf{v})$ can be parametrised as $\frac{\mathrm{d}\sigma}{\mathrm{d}E_R}(E_R, \mathbf{v}) = \frac{1}{v^2}(\sum_n a_n v^n)$, according to the approach developed in [26]. The interactions generically considered for the interpretation of the dark matter experimental results correspond to $n = 0$.

TABLE I. – *Combination of DAMA/LIBRA Phase-I and Phase-II results. In the third column also DAMA/NaI data are included. In the analysis here reported, the period is left as free parameter. For the complete discussion of the results see* [29].

	Phase-I + Phase-II	DAMA/NaI + Phase-I + Phase-II
Total exposure:	2.17 tonne $\times$ yr	2.46 tonne $\times$ yr
Statistical significance:	12.0σ	12.9σ
Period:	(0.9987 $\pm$ 0.0008) yr	(0.9987 $\pm$ 0.0008) yr
Phase:	(May, 25th $\pm$ 5 days)	(May, 25th $\pm$ 5 days)
Amplitude of modulation:	(0.0096 $\pm$ 0.0008) cpd/kg/keV	(0.0103 $\pm$ 0.0008) cpd/kg/keV

As a consequence of the composition of velocities in eq. (2), the differential rate acquires a periodic time dependence, with a period of one year. The Fourier expansion is

$$(4) \qquad \frac{\mathrm{d}R}{\mathrm{d}E_R} = A_0 + \sum_{n=1}^{\infty} A_n \cos n\omega(t - t_0) + \sum_{n=1}^{\infty} B_n \sin n\omega(t - t_0),$$

where A_n and B_n are Fourier coefficients, $\omega = 2\pi/T$, with $T = 1$ year, and t_0 is a reference time. Higher order harmonics decrease as $\epsilon^n = (V_\oplus/v_\odot)^n$ [25] and, if t_0 is the time of maximum of $\mathbf{v}_{obs}(t)$ (eq. (2)) and for isotropic velocity distribution, $B_n = 0$ [27]. Therefore, in first approximation, $\frac{\mathrm{d}R}{\mathrm{d}E_R} = A_0 + A_1 \cos \omega(t - t_0)$, where A_0 is the constant differential rate and A_1 is the amplitude of the modulation. The phase of the modulation depends on the time of maximum and minimum rate during the year, strictly related to the time of maximum and minimum velocity distribution, that has been shown to be a function of v_{min} [27] and of the type of interaction [28].

3. – The COSINUS project: Scientific motivation

3˙1. *Annual modulation in DAMA/LIBRA*. – The DAMA/LIBRA experiment is an array of 25 scintillating NaI(Tl) crystals (total mass $\simeq$250 kg), operated at room temperature and located in Gran Sasso National Laboratory (LNGS), Italy. It is designed for the direct detection of the dark matter event rate annual modulation [1]. Recently the DAMA/LIBRA Collaboration released new data, collected over six annual cycles [29], which confirm the previous claims [30] of detection of a signal consistent with the hypothesis of dark matter particles in the galactic halo (see table I).

3˙2. *Experimental panorama*. – The interpretation of the time-dependent signal detected by DAMA/LIBRA as the signature of dark matter particles suffers from the evidence of the other experimental null-results [5-13]. The analysis of the region of parameters identified or excluded by the data is in general performed in an arbitrary, theoretical framework, common to all the experiments. It consists in assuming the dark matter velocity in the halo distributed as the Maxwell-Boltzmann function discussed in sect. **2**, with $v_0 = 220$ km/s and $v_{esc} = 544$ km/s, and the local dark matter mass density at the Solar System location equal to $\rho_\chi = 0.3$ GeV/cm^3. The differential dark matter-nucleus cross section is computed for an elastic scattering, proportional to $1/v^2$, where v is the relative velocity between the incoming dark matter particle and the target nucleus.

The assumed interaction selects the nuclear response function involved, that, in the case of spin-independent elastic scattering and of isospin conserving interactions (*i.e.*, equal for protons and neutrons), is proportional to the atomic mass number squared. If the nuclear angular momentum is different from zero, also spin-dependent cross sections can be considered. Within these scenarios, the region of parameters identified by DAMA is above the upper limits achieved by the other experiments [5-13]. However, the DAMA signal remains a statistically robust and unexplained excess in agreement with expectations. It has motivated the elaboration of halo- and model-independent methods for the comparison with other experimental results. Despite the effort, a reconciling region of parameters up to date has not been found [14, 15]. However its interpretation as a dark matter signature cannot be ruled out because of the wide range of still open scenarios and the lack of a decisive alternative explanation. The COSINUS experiment has the potential to provide definitive answers to this long-standing question.

$3^\cdot3$. *The COSINUS project*. – The Cryogenic Observatory for SIgnatures seen in Next-generation Underground Searches (COSINUS) consists in the development of a cryogenic calorimeter based on radiopure NaI crystals operated at $O(10\,\mathrm{mK})$ temperature. The initial R&D phase was funded by the National Scientific Committee, group 5 (CSN5) of INFN, for three years of prototype development, from 2016 to 2018 [31] and one year prolongation to 2019 was recently approved. Starting in 2019, a Max Planck Research Group Grant has been assigned, with the duration 5 years, for the realisation of COSINUS from an R&D project to an experiment.

Other NaI-based experiments share the COSINUS urgency of reproducing the DAMA setup for testing the annual modulation signal. In terms of detection principle COSINE-100 [20], ANAIS-112 [21], SABRE [22], PICO-LON [23] and DAMA/LIBRA [1], are single channel experiments: any event, both electron and nuclear recoils, manifests as scintillation light and the discrimination of the signal from background relies on the time dependence of the count rate over the year. COSINUS aims at a dual channel detector, which collects both the light and the heat produced by a particle interaction in the crystal. The discrimination of e^-/γ events from nuclear recoils can provide a powerful test of the nature of the DAMA signal.

4. – Experimental concept

$4^\cdot1$. *Detector setup*. – The COSINUS prototype design consists of a small cubic NaI crystal, resting on a thin disc of a harder material (*e.g.*, CdWO$_4$) named carrier, of about $4\,\mathrm{cm}$ in diameter and $\sim$1–2 mm of thickness, which hosts the Transition Edge Sensor (TES), the temperature sensor. Epoxy resin or silicone oil make an interface between the cubic NaI crystal and the carrier. The crystal is enclosed in a silicon beaker of about 4–5 cm of diameter and height and about $600\,\mu\mathrm{m}$ of wall thickness, also instrumented with a TES. The interactions of a particle inside the NaI volume produce both heat, which is dissipated by phonon propagation, that is by vibrations of the crystal lattice, and scintillation light. The NaI crystal, interfaced to the carrier and the TES, is the phonon detector. The phonon detector foresees a carrier for the TES instead of a direct evaporation because the NaI is hygroscopic and makes difficult the application of the TES on its surface. The silicon beaker, instrumented with a second TES, constitutes the light detector. The silicon beaker serves as absorber for the scintillation light and the beaker shape is chosen to achieve a good light absorption, necessary because the amount of deposited energy going into the production of light is in general only a few %. The

carrier and the light absorber are designed to optimise the active surrounding coverage, which works as background veto for α-induced–surface events. For this purpose the carrier disc diameter exceeds the crystal dimensions and fits the silicon beaker diameter. The detection of both heat and light is at the basis of the particle discrimination provided by cryogenic scintillating calorimeters, since, unlike room temperature scintillators, they can measure the phonon signal, which makes the largest part of the detected signal ($\simeq 90\%$). The energy directly converted in phonons allows to reconstruct the incoming particle energy, because it is almost independent of the particle type. The amount of emitted light is instead a function of the particle nature, because of the phenomenon of light quenching. The ratio between the two signals, that is between the light energy and the phonon energy, called Light Yield (LY), allows the discrimination between e^-/γ events and nuclear recoil events and, to some extent, even between recoils off Na and I.

4$\cdot$2. *TES: Superconducting thermometer*. – The Transition Edge Sensor (TES) is a superconducting thermometer. It is a thin film of metal, operated within its superconducting and normal conducting phase transition. Small variations in temperature ($\mathcal{O}(\mu\,\mathrm{K})$) cause a steep increase of the TES resistance ($\mathcal{O}(\mathrm{m}\Omega)$), which is registered by Superconducting Quantum Interference Device (SQUID) amplifiers.

4$\cdot$3. *Performance simulation*. – The COSINUS prototype performance was simulated and discussed in [31]. In fig. 1 the simulated events in the LY energy plane are shown, where the LY is the ratio between the light and the phonon energy. The solid lines identify the LY region where 80% of the events of the respective event class are expected. The e^-/γ band is centered at $\sim$1 by definition. The background has been fixed to $1\,\mathrm{cpd}/\,\mathrm{kg}/\,\mathrm{keV}$, plus a concentration of $^{40}\mathrm{K}$ of 20 ppb, according to the DAMA/LIBRA upper limit reported in [1]. The electron capture (EC) of $^{40}\mathrm{K}$ nuclei to $^{40}\mathrm{Ar}$ [32, 33]
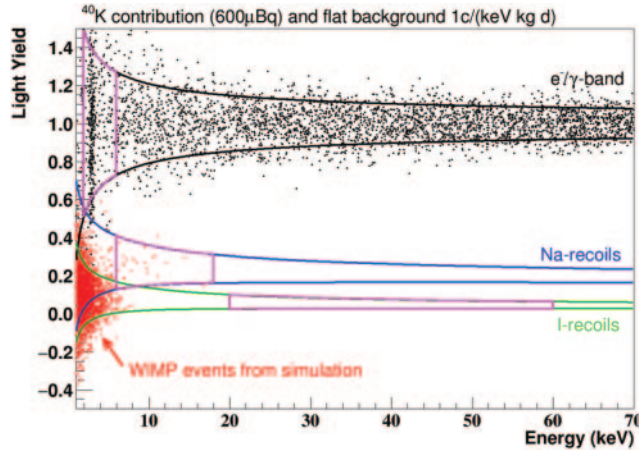

Fig. 1. – Simulated distribution of background and signal events in the Light Yield *vs.* Energy (keV) plane. From top to bottom: e^-/γ band (black), sodium (blue) and iodine (green) recoil bands. The bands confine the region where 80% of the events of the respective event class are expected. Dots mainly distributed in the iodine band are simulated WIMP events, assuming a dark matter mass of $10\,\mathrm{GeV}/c^2$ and $\sigma = 2\cdot 10^{-4}$ pb, according to an analysis of DAMA data performed in the standard scenario [34]. At around 3 keV, the spectral line from the atomic relaxation of the simulated concentration of $^{40}\mathrm{K}$ (K-shell emission) is evident.

is followed by atomic relaxation. This latter mainly occurs by emitting X-rays and Auger electrons from the K-shell at energy around 3.2 keV which falls in the Region Of Interest (ROI) of DAMA signal, and by emitting γ-rays at $\simeq 1.5$ MeV if ^{40}Ar is left in its first excited state. The potassium low energy emission is clearly visible as a line in the e^-/γ band. On top of background, a WIMP signal for a dark matter particle mass of 10 GeV$/c^2$ and a scattering cross section $\sigma_0^{SI} = 2 \times 10^{-4}$ pb is simulated, in agreement with an interpretation of the DAMA finding in the standard scenario [34]. The WIMP events appear at low energies mostly in the iodine band and at high energy in the sodium band, for kinematic reasons. A total of 2386 events are found in the nuclear band, in the energy window (1–6) keV. About 45% of these events falls in the (1–2) keV region, due to the exponential behaviour of the dark matter recoil spectrum. This shows the advantage of a low threshold detector.

5. – COSINUS prototypes: Measured data

The first and second COSINUS prototypes have been tested in the Max Planck Institute cryogenic test facility installed deep underground in the Gran Sasso National Laboratory (Italy).

5˙1. *Pulse shape*. – The pulse formation depends on the transmission of phonons propagating in the crystal lattice to the TES. The time dependence of the thermometer response is formalised and tested in [35]. Equation (5)(^{1}) has been shown to be a good model of the time dependence of the detected pulse. $\Delta T_e(t)$ is the temperature variation of the electrons in the thermometer, that is the heating experienced by the TES as consequence of the coupling between electrons and phonons. High frequency phonons undergo ballistic propagation across the crystal and flow to the TES, where they thermalise via electron interactions. This is the non-thermal component of the pulse, described by the term proportional to A_n in eq. (5), where τ_n is the constant time of the phonon thermalisation and τ_{in} is the intrinsic time of relaxation of the thermometer. A second signal is produced by the thermalised phonon flow to the absorber, which can be detected again by the thermometer as a slow component. This is described by the term proportional to A_t, where τ_t is the thermal relaxation time of the absorber:

$$(5) \qquad \Delta T_e(t) = \Theta(t)[A_n(e^{-t/\tau_{in}} - e^{-t/\tau_n}) + A_t(e^{-t/\tau_t} - e^{-t/\tau_n})].$$

The description of the pulse shape according to eq. (5) is in agreement with the signals resulting by many different crystals; however, the employment of sodium iodide crystals has put into evidence a different pulse shape [36]. In fig. 2, a pulse obtained by averaging several events in the NaI from an ^{241}Am source is shown. The method applied to obtain a good fit of the pulses consists in adding an additional 2nd thermal component in eq. (5), but a physical explanation is still missing. Further studies for elaborating a pulse shape model in NaI-based cryogenic detectors are still ongoing.

5˙2. *COSINUS 2nd prototype*. – The dimension and the performance parameters of the second COSINUS prototype are summarised in table II. The Light Yield *vs.* Energy plane in fig. 3 shows data distributed according to two populations: an e^-/γ band centered around LY $\simeq 1$ and a population of events around LY $\simeq 0$, attributed to the

---

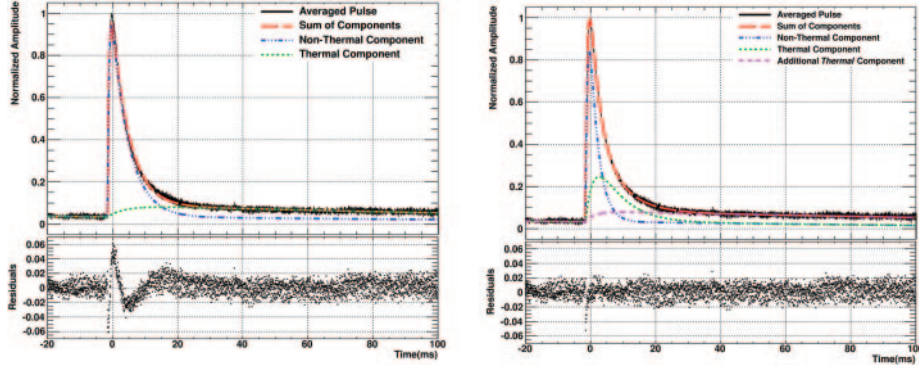(^{1}) Equation (5) corrects a sign in eq. (10) of [35] in the term of the non-thermal component.

Fig. 2. – Fit of a standard event obtained by averaging a large number of 60 keV X-ray events from ^{241}Am source, performed with the two-component function in eq. (5) (left panel) and with an additional 2nd thermal component (right panel). On the bottom, the residuals are shown.

carrier. This second population is mainly attributed to stress in the materials, which showed cracks during the unmounting, and also to particle events which released energy directly in the carrier. In the e^-/γ band the discrimination of the atomic radiation from ^{40}K is evidently confirmed, together with the 60 keV line from an ^{241}Am source. A relevant result is the discrimination of another atomic spectral line, that is the iodine escape line at around 30 keV, resulting from the photoelectric interaction of the 60 keV X-rays of the ^{241}Am source with the iodine K-shell electrons. The iodine K-shell binding energy is $\simeq 33$ keV. This result has a noteworthy implication. The most abundant isotope of iodine is ^{127}I and it has a large cross section ($\sigma \simeq 10$ barns for thermal neutrons [37]) for the (n,γ) process which leads to ^{128}I production. ^{128}I is unstable and decays to ^{128}Xe via β^--decay ($\sim 93.1\%$) and to ^{128}Te via electron capture (EC) ($\sim 6.9\%$) or via β^+-decay ($\sim 0.0026\%$), with half-life $\tau_{1/2} = 24.99$ min [32, 33]. ^{128}Te is left on its first nuclear excited state or on its ground state. In the first case, an X-ray emission at $\simeq 743.22$ keV is expected for nuclear de-excitation. The electron capture is followed by an atomic relaxation occurring through X-ray and Auger emissions, which are likely to be detected as the binding energies of the atomic shells (*e.g.*, $\simeq 33$ keV and $\simeq 4.5$ keV, for K and L$_3$-shells, respectively, [32]), whose intensities can be found in [39]. Single atomic spectral lines could emerge if the ^{128}I production process occurred on the crystal surface. COSINUS has proven to have the chance for discriminating also this background.

TABLE II. – *COSINUS 2nd prototype parameters* [38].

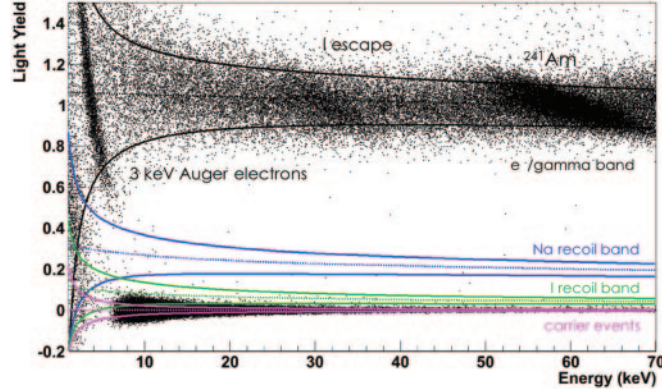|	
Mass:	$\simeq 66$ g
Exposure:	1.32 kg days
Crystal dimension:	$(20 \times 20 \times 30)$ mm^3
Interface:	Epoxy resin
Phonon detector threshold:	$[8.62 \pm 0.02$ (stat.)] keV (baseline energy resolution $\sigma = 1.01$ keV)
Light detector threshold:	0.6 keV$_{ee}$ (baseline energy resolution $\sigma = 0.015$ keV$_{ee}$)
Energy detected in light:	$\simeq 13\%$

Fig. 3. – COSINUS 2nd prototype data, shown in the Light Yield *vs.* Energy plane. From top to bottom: e^-/γ band (black), the sodium recoil band (blue), the iodine recoil band (green) and the carrier band (magenta). ^{40}Ar K-shell line and the ^{128}I escape line are visible at $\simeq 3.2$ keV and $\simeq 30$ keV, respectively. More details are in the text. At 60 keV the line from ^{241}Am source is visible. The carrier band is populated by particles interacting with the carrier volume itself and, mainly, by lattice vibrations due to cracks that in this measurement occurred in the NaI and the carrier due to thermal stress induced by the Epoxy resin-based interface.

6. – Prototype development: Status

From 2016 to 2018 COSINUS has run several different prototypes to achieve the optimal performance. In table III the main steps are listed. The first prototype measurement represents the first time a NaI crystal was successfully operated as cryogenic detector. The linearity between the light and the phonon energy was experimentally proven. The peculiar behaviour of the pulse shape discussed above was encountered for the first time [36]. The second prototype, as discussed in sect. **5** was the first realisation of the COSINUS light detector design, with the silicon beaker-shaped absorber, which showed a performance well beyond the expectations, since the goal was $\simeq 4\%$ [38]. From the 4th prototype on, several NaI crystals have been produced by SICCAS, whose collaboration with COSINUS was formally established. The new batch of NaI/NaI(Tl) crystal from SICCAS is currently employed in the COSINUS tests for detector development.

TABLE III. – *Chronology of the main COSINUS prototype developments. LD: Light Detector. PD: Phonon Detector. The column "Interface" specifies the material used for the NaI/carrier interface, where the carrier is the crystal carrying the TES. Wafer SOS stays for wafer of Silicon-On-Sapphire, initially used as light absorber.*

Prototype	LD	PD	Interface	Light collection	PD threshold
1st (2016)	wafer SOS	NaI	Silicone oil	$\simeq 3.7\%$	10 keV
2nd (2016/17)	Si beaker	NaI	Epoxy resin	$\simeq 13\%$	8.3 keV
3rd (2017)	”	”	Silicone oil	”	6.5 keV
4th → 11th (2017/18)	”	NaI(Tl)	”	Work ongoing	

6˙1. *Quenching factors*. – The evidence that different class of particles interacting in the crystal volume produce different amount of scintillation light is empirically described by the Birks' law [40]. According to the Birks' law, heavier projectiles produce less scintillation light and the factor of suppression is commonly called Quenching Factor (QF). Knowledge of quenching factors is extremely important for particle discrimination because it allows the reconstruction of the deposited energy and the identification of the e^-/γ band and the nuclear recoil bands. The QF measurement can be performed via calibration with neutron sources in underground facilities as well as via calibration with a mono-energetic source of neutrons at accelerator facilities. A systematic study to establish the optimal concentration of thallium to be used as NaI dopant is being performed at the Meier-Leibnitz Laboratorium (MLL), where a Tandem-van-de-Graaf accelerator produces and accelerates ^{11}B ions, that if addressed to a cell of pressurised hydrogen, provide a mono-energetic beam of 11 MeV neutrons. COSINUS already ran two measurements at the MLL, one on a NaI(pure) crystal in April 2018, and one on a NaI(Tl) crystal, in November 2018. Interpretation of results is challenging, therefore further investigations to clarify and achieve a definitive explanation are mandatory.

7. – Conclusion

A halo model and interaction independent check of the DAMA detection is mandatory either for adding a fundamental brick to the building of a dark matter theory or to unravel the origin of the signal which has been conditioning both the theoretical and experimental search for dark matter particles for many years. COSINUS is a sodium iodide based cryogenic calorimeter and aims at participating to this study with a powerful technique which can provide a target-independent cross-check of the DAMA signal, clarifying its nature thanks to the discrimination of e^-/γ events from nuclear recoils.

* * *

REFERENCES

[1] DAMA COLLABORATION (BERNABEI R. *et al.*), *Nucl. Instrum. Methods A*, **592** (2008) 297, arXiv:0804.2738.

[2] BERTONE G. and HOOPER D., *Rev. Mod. Phys.*, **90** (2018) 045002, arXiv:1605.04909.

[3] DAMA COLLABORATION (BERNABEI R. *et al.*), *Nucl. Phys. B - Proc. Suppl.*, **70** (1999) 79.

[4] DAMA COLLABORATION (BERNABEI R. *et al.*), arXiv:1805.10486 (2018).

[5] XENON COLLABORATION (APRILE E. *et al.*), *Phys. Rev. Lett.*, **121** (2018) 111302, arXiv:1805.12562.

[6] LUX COLLABORATION (AKERIB D. S. *et al.*), *Phys. Rev. Lett.*, **118** (2017) 021303, arXiv:1608.07648.

[7] PICO COLLABORATION (AMOLE C. *et al.*), *Phys. Rev. Lett.*, **118** (2017) 251301, arXiv:1702.07666.

[8] SuperCDMS COLLABORATION (AGNESE R. *et al.*), *Phys. Rev. Lett.*, **120** (2018) 061802, arXiv:1708.08869.

[9] SUPERCDMS COLLABORATION (AGNESE R. et al.), *Phys. Rev. D*, **97** (2018) 022002, arXiv:1707.01632.

[10] PANDAX-II COLLABORATION (TAN A. et al.), *Phys. Rev. Lett.*, **117** (2016) 121303, arXiv:1607.07400.

[11] DARKSIDE COLLABORATION (AGNES P. et al.), *Phys. Rev. Lett.*, **121** (2018) 081307, arXiv:1802.06994.

[12] CRESST-II COLLABORATION (ANGLOHER G. et al.), *Eur. Phys. J. C*, **74** (2014) 3184, arXiv:1407.3146.

[13] EDELWEISS COLLABORATION (ARMENGAUD E. et al.), *JCAP*, **05** (2016) 019, arXiv:1603.05120.

[14] GONDOLO P. and GELMINI G. B., *JCAP*, **12** (2012) 015, arXiv:1202.6359.

[15] CATENA R. and GONDOLO P., *JCAP*, **09** (2014) 045, arXiv:1405.2637.

[16] PRADLER J., SINGH B. and YAVIN I., *Phys. Lett. B*, **720** (2013) 399, arXiv:1210.5501.

[17] PRADLER J. and YAVIN I., *Phys. Lett. B*, **723** (2013) 168, arXiv:1210.7548.

[18] RALSTON J. P., arXiv:1006.5255 (2010).

[19] BERNABEI R. et al., *Eur. Phys. J. C*, **74** (2014) 3196, arXiv:1409.3516.

[20] COSINE-100 COLLABORATION (ADHIKARI G. et al.), *Eur. Phys. J. C*, **78** (2018) 107, arXiv:1710.05299.

[21] ANAIS COLLABORATION (AMARÉ J. et al.), *J. Phys. Conf. Ser.*, **718** (2016) 042052, arXiv:1512.04239.

[22] SABRE COLLABORATION (TOMEI C.), *Nucl. Instrum. Methods A*, **845** (2017) 418.

[23] PICO-LON COLLABORATION (FUSHIMI K. I. et al.), *JPS Conf. Proc.*, **11** (2016) 020003, arXiv:1605.04999.

[24] DRUKIER A. K., FREESE K. and SPERGEL D. N., *Phys. Rev. D*, **33** (1986) 3435.

[25] LEE S. K., LISANTI M. and SAFDI B. R., *JCAP*, **11** (2013) 033, arXiv:1307.5323.

[26] FITZPATRICK A. L., HAXTON W., KATZ E., LUBBERS N. and XU Y., *JCAP*, **02** (2013) 004, arXiv:1203.3542.

[27] FREESE K., LISANTI M. and SAVAGE C., *Rev. Mod. Phys.*, **85** (2013) 1561, arXiv:1209.3339.

[28] DEL NOBILE E., GELMINI G. B. and WITTE S. J., *JCAP*, **02** (2016) 009, arXiv:1512.03961.

[29] BERNABEI R. et al., *Nucl. Phys. At. Energy*, **19** (2018) 307, arXiv:1805.10486.

[30] DAMA COLLABORATION (BERNABEI R. et al.), *Eur. Phys. J. C*, **56** (2008) 333, arXiv:0804.2741.

[31] ANGLOHER G. et al., *Eur. Phys. J. C*, **76** (2016) 441, arXiv:1603.02214.

[32] FIRESTONE R. B. and SHIRLEY V. S., *Table of Isotopes*, eighth edition, (Wiley-VCH) 1998.

[33] https://www.nndc.bnl.gov.

[34] SAVAGE C., GELMINI G., GONDOLO P. and FREESE K., *JCAP*, **04** (2009) 010, arXiv:0808.3607.

[35] PRÖBST F., FRANK M., COOPER S. et al., *J. Low Temp. Phys.*, **100** (1995) 69.

[36] COSINUS COLLABORATION (ANGLOHER G. et al.), *JINST*, **12** (2017) P11007, arXiv:1705.11028.

[37] https://www.oecd-nea.org/janisweb.

[38] SCHÄFFNER K. et al., *J. Low. Temp. Phys.*, **193** (2018) 1174.

[39] https://www.nndc.bnl.gov/ensdf/EnsdfDispatcherServlet.

[40] BIRKS J. B., *International Series of Monographs on Electronics and Instrumentation*, Vol. **27** (Macmillan, New York) 1964.